

# Effects of index angle on flow ripple of a tandem axial piston pump<sup>\*</sup>

Bing XU<sup>†</sup>, Shao-gan YE, Jun-hui ZHANG

(The State Key Laboratory of Fluid Power Transmission and Control, Zhejiang University, Hangzhou 310027, China)

<sup>†</sup>E-mail: bxu@zju.edu.cn

Received Oct. 12, 2014; Revision accepted Jan. 27, 2015; Crosschecked Apr. 13, 2015

**Abstract:** A high noise level is one of the prominent shortcomings of an axial piston pump which is widely used in industrial and mobile applications. In this paper, a simulation model of an axial piston pump is developed based on a single piston chamber model, for capturing the dynamic characteristics of the discharge flow rate. The compressibility of fluid and main leakages across different friction pairs are considered. The simulation model is validated by a comparison of discharge flow ripple with the measured results using the secondary source method. The main cause of flow ripple is identified by a comparison of the frequency spectrums of actual and kinematic flow ripples. Flow rates with different index angles are analyzed in time and frequency domains. The findings show that an index angle of 20° is the most effective in reducing the flow ripple of a tandem axial piston pump, because the frequency contents at odd harmonics can be cancelled out. A sensitivity analysis is conducted at different pressure levels, speeds, and displacement angles, which reveals that with an index angle of 20°, the sensitivity of flow ripple can be reduced by almost 50% over a wide variety of working conditions.

**Key words:** Axial piston pump, Flow ripple, Index angle, Sensitivity analysis

doi:10.1631/jzus.A1400309

**Document code:** A


**CLC number:** TH13

## 1 Introduction

Axial piston pumps are widely employed in industrial and mobile applications for their compactness, reliability, and efficiency. In contrast to their advantages, high noise levels are their disadvantages. In an axial piston pump, the noise can be divided into fluid-borne noise and structure-borne noise (Fiebig, 2001). Fluid-borne noise originates from flow ripple, which is generated by the limited number of pistons and fluid compressibility. Structure-borne noise originates from the internal forces and moments, which are generated by varying piston chamber pressures and their varying acting points.

Many methods have been devised in attempts to reduce pump noise. Edge and Darling (1989) used a heavily damped check valve to reduce the flow ripple of an axial piston pump. Manring (2003) investigated the principal advantages of using three different types of slot geometry (constant area, linear varying, and quadratically varying slot geometries). A recommendation was also made for choosing the slot geometry when the pump is designated for use in a low displacement angle. Seeniraj and Ivantysynova (2011) optimized the valve plate compression and decompression regions with a multi-objective optimization method using genetic algorithm, considering the noise and volumetric efficiency. Johansson *et al.* (2002) investigated the impacts of cross-angle on flow ripple and also developed an optimization methodology to optimize the cross-angle. The influences of the cross-angle on internal forces and moments were investigated (Johansson *et al.*, 2001; 2003). An experimental study was also conducted to identify the benefits of the cross-angle. The results

<sup>\*</sup> Project supported by the National Basic Research Program (973) of China (No. 2014CB046403), and the Zhejiang Provincial Natural Science Foundation of China (No. LQ14E050005)

 ORCID: Bing XU, <http://orcid.org/0000-0003-0236-7896>

© Zhejiang University and Springer-Verlag Berlin Heidelberg 2015

indicated that the cross angle is beneficial when used in a constant pressure regulated pump (Johansson *et al.*, 2007). Ericson *et al.* (2007; 2008) investigated the possibility of applying cross-angle design to an axial piston motor, and a complex method was used to optimize the cross-angle. Nafz *et al.* (2012) used a variable reversing valve to control the valve openings, which can be adjusted according to actual working conditions. In their study, two different strategies (a flow ripple strategy and a swash plate torque ripple strategy) were adopted to control the valve openings and were found to be effective in reducing the noise of the axial piston pump. Huang *et al.* (2014) optimized the valve plate of an asymmetric axial piston pump to reduce flow ripple. Most of these investigations focused on reducing flow ripple and pulsations of internal forces and moments, but none of them took the shaft torque ripple into consideration.

Recently, laboratory experiments have suggested that the noise produced by an axial piston pump is directly related to the shaft torque ripple (Landsberger, 2003). Based on this finding, Manring *et al.* (2007) investigated the shaft torque ripple of a tandem pump theoretically. Their results showed that an index angle of  $10^\circ$  was the most effective in reducing the torque ripple for a tandem axial piston pump using nine pistons within one rotating group. Also, the torque amplitude can be reduced by about 75%. Mehta (2006) concluded that the flow ripple in the discharge line can also be reduced most when the index angle is  $10^\circ$ . However, these two investigations took only the kinematic torque and flow ripples into consideration. The fluid compressibility and leakages across different friction pairs were neglected. In reality, the flow ripple generated by the dynamics of hydraulic oil and the design of the valve plate is more complex than the kinematic component. This implied that a further investigation was necessary to capture fully the effects of index angle on the generation of flow ripple.

This paper presents the flow ripple characteristics of a tandem axial piston pump using nine pistons within one rotating group with different index angles. The remainder of this paper comprises the following:

1. A dynamic simulation model of an axial piston pump is built, based on a single piston chamber model, for capturing the flow ripple characteristics.

The model considers fluid compressibility and main leakages across different friction pairs in the axial piston pump and is validated by a comparison of discharge flow ripple with experimental tests using the secondary source method.

2. The causes of flow ripple are identified by a comparison of actual and kinematic flow ripples. The flow ripples of the tandem axial piston pump are compared with different index angles at the rated working condition. The optimal index angle is identified that can obtain the smallest flow ripple.

3. A sensitivity analysis is performed to analyze the sensitivity of flow ripple to different pressure levels, speeds, and displacement angles.

## 2 Dynamic simulation model

### 2.1 Description of the tandem pump

A simplified tandem pump is shown in Fig. 1 with specifications listed in Table 1 (Ye *et al.*, 2014). The tandem pump includes two identical rotating groups, which are connected to one shaft. Because the swash plate inclines several degrees, the piston reciprocates along the  $z$  axis when the shaft rotates around the  $z$  axis. When the piston leaves the piston chamber, fluid is sucked into the piston chamber,

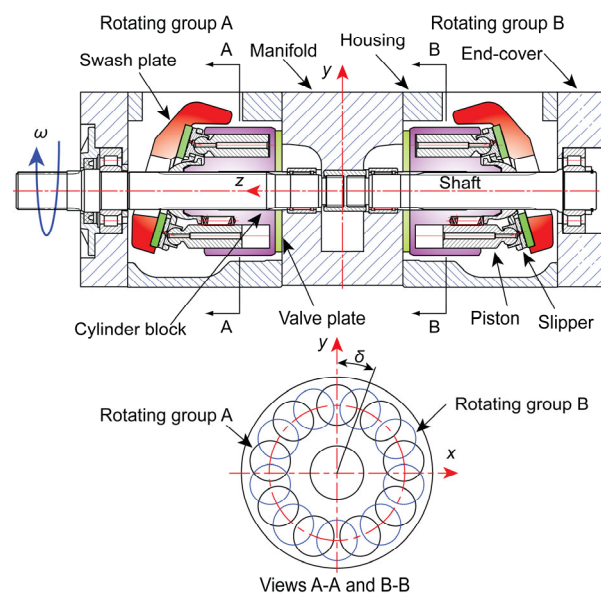


**Fig. 1 Schematic of a tandem pump (Reprinted from (Ye *et al.*, 2014) with modification, Copyright 2014, with permission from ASME)**

**Table 1 Specifications of the tandem axial piston pump**

Feature	Description
Displacement (cm <sup>3</sup> /r)	2×71
Number of pistons	2×9
Dimension (mm×mm×mm)	702×208×284
Inlet pressure (open circuit) (MPa)	≤0.08
Outlet pressure (MPa)	≤28
Speed range (r/min)	≤2200
Variable	Yes

and is delivered to the discharge port when the piston enters into the piston chamber. The two rotating groups suck fluid from the same suction port and delivered fluid to the same discharge port. Views A-A and B-B of Fig. 1 show a sectional view taken through the cylinder block of rotating groups A and B. For each rotating group, the cylinder block is indexed relative to the other by an index angle of  $\delta$  when the tandem pump is assembled (Manring *et al.*, 2007). For simplicity, the control mechanism is not shown. The suction and discharge ports are manufactured in the manifold, which cannot be seen from this view.

## 2.2 Simulation model

The dynamic model for one rotating group (Fig. 2a) is composed of several single piston chamber models (Fig. 2b) (Ye *et al.*, 2014). The pressure in the piston chamber is determined using the control volume method (Ivantysyn and Ivantysynova, 2003). The pressure is affected by leakages across different friction pairs, such as the piston/cylinder pairs, slipper/swash-plate pairs, and cylinder/valve-plate pair. The rate of pressure in the piston chamber is expressed as

$$\frac{dp}{dt} = \frac{K_e}{V_{pc}} \left( Q_{lp} - Q_{hp} - Q_l - \frac{dV_{pc}}{dt} \right), \quad (1)$$

where  $p$  denotes the pressure in the piston chamber,  $K_e$  is the bulk modulus of hydraulic oil,  $V_{pc}$  is the volume of the piston chamber,  $Q_{lp}$  and  $Q_{hp}$  are the flow rates between the piston chamber and the suction and discharge ports, respectively, and  $Q_l$  is the leakage.

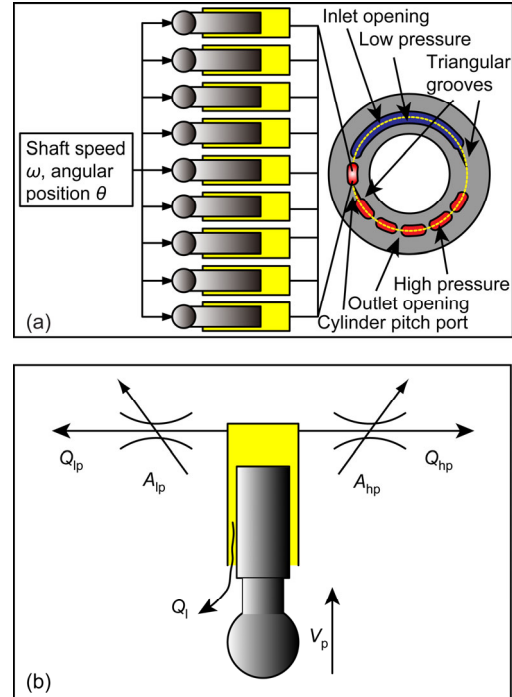
The flow rates between the piston chamber and the suction and discharge ports are calculated for

turbulent flow through the simple throttle orifice using

$$Q_{lp} = CA_{lp} \sqrt{\frac{2|p - p_l|}{\rho}} \cdot \text{sign}(p - p_l), \quad (2)$$

$$Q_{hp} = CA_{hp} \sqrt{\frac{2|p_h - p|}{\rho}} \cdot \text{sign}(p_h - p), \quad (3)$$

where  $C$  is the flow coefficient,  $p_l$  and  $p_h$  are the pressures in the suction and discharge ports, respectively,  $A_{lp}$  and  $A_{hp}$  are the throttle areas between the piston chamber and the suction and discharge ports, respectively, and  $\rho$  is the density of hydraulic oil.



The flow coefficient is sensitive to the flow speed which makes it hard to determine. A simulation conducted by Ma *et al.* (2010) using computational fluid dynamic technology revealed that the flow coefficient  $C$  fluctuates around 0.7. Thus, it is set as 0.7 in the simulation model. The throttle areas are calculated according to valve plate slot geometry.

The fluid volume in the piston chamber is expressed by

$$V_{pc} = V_0 - \frac{\pi}{4} d_p^2 R \tan \beta \cos \theta, \quad (4)$$

where  $V_0$  is the dead volume of the piston chamber in the outer dead center,  $d_p$  is the diameter of the piston,  $R$  is the distribution radius of the piston hole,  $\beta$  is the inclination angle of the swash plate, and  $\theta$  is the rotational angle of the cylinder.

The bulk modulus of hydraulic oil is a function of pressure and temperature, which was measured by Ma *et al.* (2010) at two temperatures and five pressure levels from 4 to 24 MPa with a step of 5 MPa. The bulk moduli at other temperatures and pressures are calculated using an interpolation method.

There are many leakage paths in a piston pump. These leakages affect not only the volumetric efficiency of the pump, but also the pressure build-up in the piston chamber. The leakage flow rates across the piston/cylinder pairs  $Q_{lc}$ , slipper/swash-plate pairs  $Q_{ls}$ , and cylinder/valve-plate pair  $Q_{lv}$  are the dominant flow losses. The total leakage considering all these leakages is calculated by (Ye *et al.*, 2014)

$$Q_l = Q_{lc} + Q_{ls} + Q_{lv}. \quad (5)$$

Considering the varying contact length and eccentricity between the piston and the piston chamber, the leakage flow  $Q_{lc}$  is expressed as

$$Q_{lc} = \frac{\pi d_p \delta_1^3}{12 \mu l_p} (1 + 1.5 \varepsilon^2) (p - p_s), \quad (6)$$

where  $\delta_1$  is the oil film thickness of the piston/cylinder pair,  $\mu$  is the dynamic viscosity of hydraulic oil,  $\varepsilon$  is the eccentricity of the piston to the piston chamber,  $p_s$  is the pressure in the pump case, and  $l_p$  is the contact length between the piston and the piston chamber, which is expressed as

$$l_p = l_0 - R \tan \beta \cos \theta, \quad (7)$$

where  $l_0$  is the contact length in the outer dead center.

The leakage flows  $Q_{ls}$  and  $Q_{lv}$  are calculated using the equation for laminar leakage flow between

two planes as expressed in Eqs. (8) and (12), respectively (Xu *et al.*, 2013; 2015).

$$Q_{ls} = \frac{C_{pb} C_{sb} C_{sp}}{C_{pb} C_{sb} + C_{pb} C_{sp} + C_{sb} C_{sp}} (p - p_s), \quad (8)$$

$$C_{pb} = \frac{\pi d_{pb}^4}{128 \mu l_{pb}}, \quad (9)$$

$$C_{sb} = \frac{\pi d_{sb}^4}{128 \mu l_{sb}}, \quad (10)$$

$$C_{sp} = \frac{\pi \delta_2^3}{6 \mu \ln(R_{sp}/r_{sp})}, \quad (11)$$

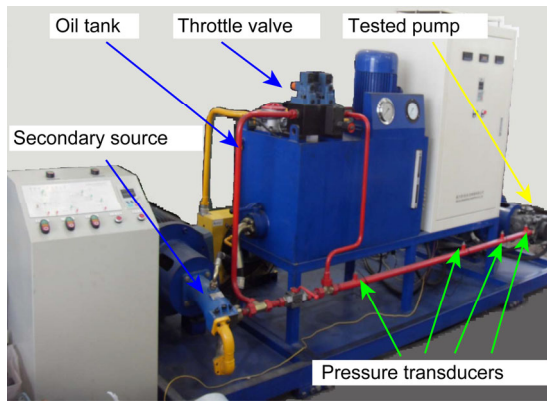
$$Q_{lv} = \frac{\alpha_f \delta_3^3}{12 \mu} \left[ \frac{1}{\ln(R_2/R_1)} + \frac{1}{\ln(R_4/R_3)} \right] (p - p_s), \quad (12)$$

where  $d_{pb}$  is the diameter of the hole in the center of the piston bore,  $l_{pb}$  is the length of the hole,  $d_{sb}$  is the diameter of the slipper hole,  $l_{sb}$  is the length of the hole in the slipper,  $\delta_2$  is the thickness of the oil film of the slipper/swash-plate pair,  $R_{sp}$  and  $r_{sp}$  are the outer and inner radii of the slipper surface, respectively,  $\delta_3$  is the thickness of the oil film of the cylinder/valve-plate pair,  $R_1$  and  $R_2$  are inner and outer radii of the inner sealing belt in the valve plate,  $R_3$  and  $R_4$  are the inner and outer radii of the outer sealing belt in the valve plate, respectively, and  $\alpha_f$  is the wrap angle of the piston chamber.

### 2.3 Validation

The internal forces and moments in an axial piston pump are difficult to be measured because of its compactness. The discharge flow ripple was measured to validate the simulation model by using the test rig shown in Fig. 3 (Ye *et al.*, 2014). Four pressure transducers with a bandwidth of 5000 Hz were mounted in the discharge line. The test rig was built according to the secondary source method (Edge and Johnston, 1990a; 1990b; ISO, 1996). The distances between the pump discharge port and each transducer were 100, 431, 898, and 1895 mm. A vane pump was used as the boost pump to prevent any unexpected phenomena in the suction port at a constant revolution speed of 1500 r/min. The speed of the test pump was limited to about 1300 r/min if the test pump worked at the maximum displacement. The

pressure was limited to about 20 MPa at the maximum displacement because the maximum power of the electric motor used to drive the tested pump was 30 kW. A pressure relief valve was used for keeping the pressure in the suction line of the test pump lower than 5 MPa, and two pressure relief valves were applied in the discharge lines of the test pump and the secondary source as safety valves. A throttle valve was used to regulate the discharge pressure of the test pump. A ball valve was used to keep the secondary source isolated from the test circuit.



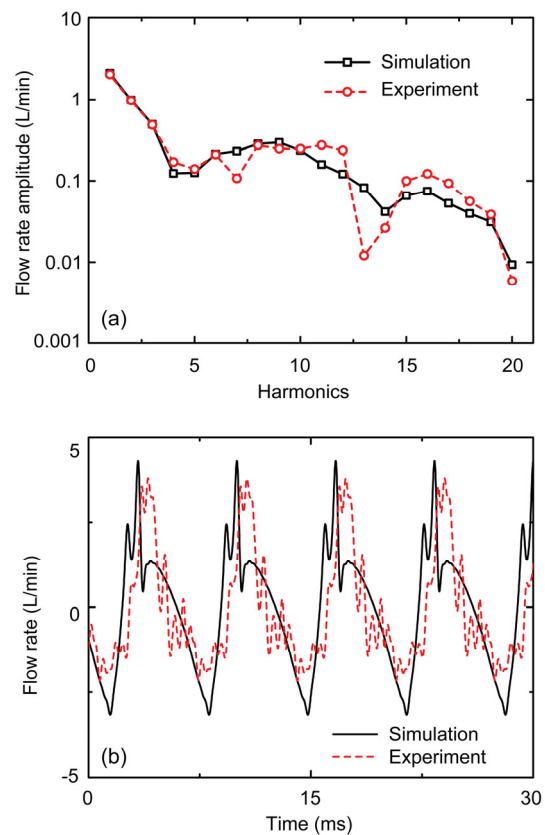
Two procedures were used to measure flow ripple. Firstly, both pressure ripples at harmonics of the test pump and the secondary source were measured, and the source impedance was calculated with pressure ripples at harmonics of the secondary source. In this study, the source impedance exhibited an anti-resonance phenomenon. A distributed-parameter model was applied to calculate the source impedance. Secondly, pressure ripples at harmonics of the test pump were measured and used to calculate the flow ripples together with the calculated source impedances.

Fig. 4 shows the measured and simulated flow ripples at a speed of 1000 r/min and a pressure level of 10 MPa in the frequency and time domains. The fundamental frequency of the secondary source was 175 Hz, and of the tested pump was 150 Hz. Thus, the 6th and 12th harmonics of the secondary source

were equal to the 7th and 14th harmonics of the test pump, respectively. The pressure ripples at these two frequencies cannot be used in the calculation of source impedance. In the frequency domain, the flow ripples at most of the harmonics agreed very well between the simulation and measurement, except the 7th and 13th harmonics, in which the experimental results were somewhat lower than those from the simulation. In the time domain, the flow rate variations from simulation and measurement showed a similar trend. The largest and lowest values were almost the same. Further, the overall flow ripple rating was calculated by

$$Q_{\text{rating}} = \sqrt{\frac{1}{2} \sum_{i=1}^N Q_i^2}, \quad (13)$$

where  $Q_i$  is the amplitude of the flow ripple at the  $i$ th harmonics, and  $N$  is the total number of harmonics.



**Fig. 4** Comparisons of simulated and measured flow rates in frequency domain (a) and time domain (b)



The overall flow ripple rating was 1.70 L/min in the experiment and 1.74 L/min in the simulation, a difference of about 2.3%. In addition, Fig. 5 shows the variation in the flow rates simulated and measured under three different working conditions. The flow ripple was lower at smaller displacements (Fig. 4b vs. Fig. 5a), higher at higher revolution speeds (Fig. 4b vs. Fig. 5b), and higher at higher pressure levels (Fig. 4b vs. Fig. 5c). The simulation results agree well with the experimental results, which indicates that the simulation model has acceptable accuracy, and thus can be used in the analysis of the performance of axial piston pumps.

### 3 Effects of index angle

#### 3.1 Flow rate from one rotating group

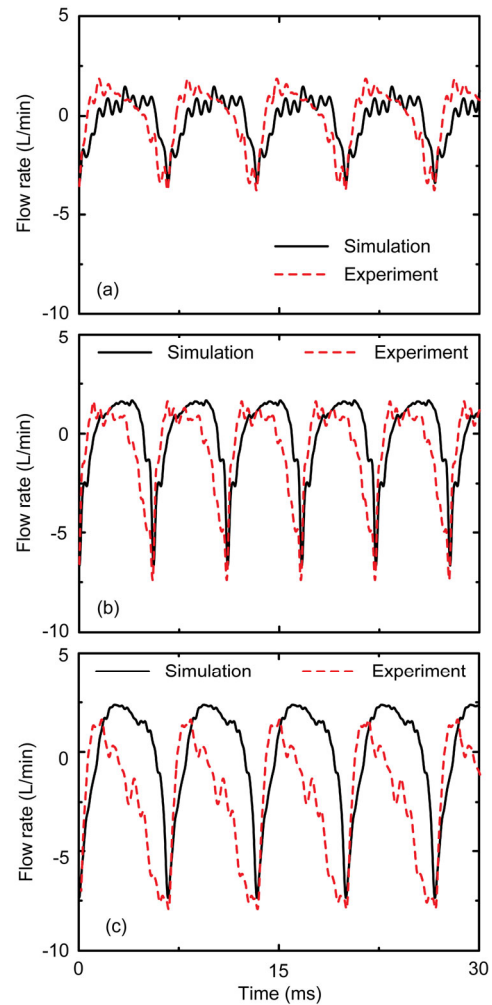
The discharge flow ripple contributes most to fluid-borne noise, because a large pressure ripple is generated as it interacts with system impedance. The pressure ripple leads to the vibration of valves and hoses in a hydraulic system, and consequently loud noise emission from these components. To investigate the impacts of index angle on the flow ripple of the tandem pump, the flow rate generated by one rotating group was investigated, as well as the factors contributing to the generation of flow ripples.

For a tandem pump, the flow rate from each rotating group can be calculated separately because it is the summation of the flow rate from all the piston chambers in each separate rotating group, given by

$$Q = \sum_{m=1}^Z Q_m, \quad (14)$$

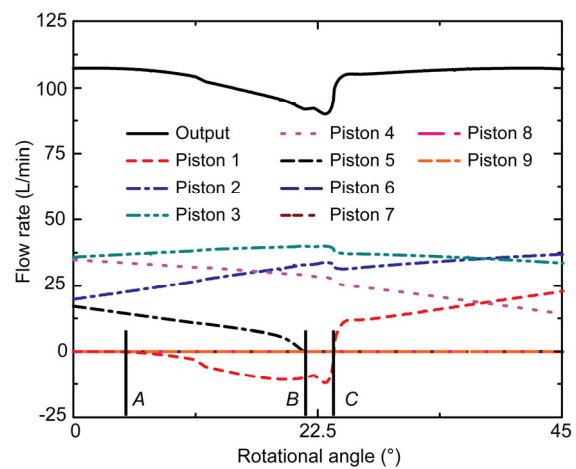
where  $Q_m$  is the flow rate from the  $m$ th piston chamber, and  $Z$  is the total number of pistons within one rotating group.

Fig. 6 shows the variation in the total discharge flow rate and the flow rate from each piston chamber for one rotating group. Although there are nine pistons, only four or five are connected to the discharge port (Fig. 7). The flow rates from pistons 6–9 are zero during this period. Before piston 1 starts connecting with the discharge port at point A (Fig. 6), there are four other pistons (pistons 2–5) connecting



**Fig. 5 Comparisons of simulated and measured flow rates under different working conditions**

(a) 50% displacement; (b) 1200 r/min; (c) 20 MPa



**Fig. 6 Variation in the total discharge flow rate and the flow rate from each piston chamber**

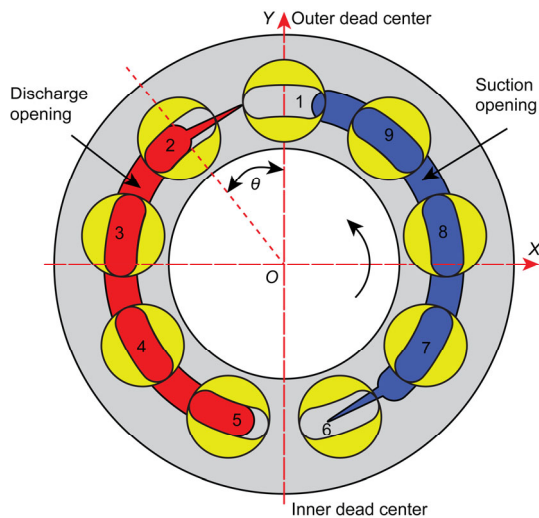


Fig. 7 A schematic diagram showing the pumping process

with the discharge port. During this period, the discharge flow rate is the summation of the flow rate from pistons 2–5. As piston 1 starts connecting with the discharge port at point A, the fluid is discharged from the discharge port into piston chamber 1. This decreases the flow rate in the discharge port. At point B, piston 5 starts losing connection with the discharge port. Then there are only four pistons (pistons 1–4) connecting with the discharge port. In addition, only three pistons (pistons 2–4) discharge fluid to the discharge port, while piston 1 keeps sucking fluid into piston chamber 1. At point C, piston 1 starts discharging fluid to the discharge port, and then the flow rate in the discharge port is the summation of the flow rates from four pistons (pistons 1–4).

Thus, three factors cause flow ripple in the discharge port. Firstly, the fluid discharging into the piston chamber from the discharge port causes a large reduction in the flow rate in the discharge port. This is also the main cause of flow ripple (Fig. 6). Secondly, the variation in the number of pistons which are in the process of discharging fluid also affects flow rate variation. Thirdly, the sinusoidal motion of the piston and consequently variation in the amount of flow rate from each piston chamber also has an effect. Thus, the actual flow ripple in the discharge port can be divided into compressible and kinematic components according to the mechanism of its generation. The compressible component is

generated by the compressibility of fluid and the large pressure difference between the discharge port and the piston chamber (as for piston 1), and the kinematic component is generated by the limited number of pistons and the sinusoidal motion of the pistons.

Compared with the complexity of the actual flow ripple, the kinematic flow ripple is simpler. For one rotating group using an odd number of pistons, the amplitude of the kinematic flow ripple in the frequency domain is given as (Ericson *et al.*, 2009)

$$Q(j2k\omega_0) = \frac{\pi d_p^2 R n \tan \beta}{(2Zk)^2 - 1}, \quad (15)$$

where  $n$  is the revolution speed,  $Z$  is the number of pistons,  $j$  is the complex conjugate,  $\omega_0$  is the fundamental frequency,  $\omega_0 = 2\pi/T$ ,  $T$  is the period, and  $k=1, 2, \dots$

Fig. 8 shows the frequency spectrums of the actual flow ripple and the kinematic flow ripple. Firstly, note that the amplitudes of the actual flow ripple are larger than those of the kinematic flow ripple. This implies that the compressible flow ripple is the main cause of the actual flow ripple, while the contribution of the kinematic flow ripple is small. This is clearly shown by the large decrease in discharge flow rate (Fig. 6). Secondly, at odd harmonics, the amplitudes of the kinematic flow ripple are zero, while those of the actual flow ripple are large. This implies that the actual flow ripple has contents at each harmonic, while the kinematic flow

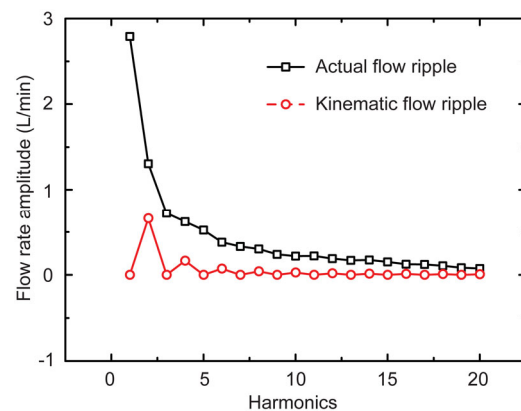


Fig. 8 A comparison of the actual flow ripple and kinematic flow ripple in the frequency domain

ripple has contents at odd harmonics. These differences between the actual and kinematic flow ripples form the basis for investigating the impacts of index angle on the flow ripple of the tandem axial piston pump.

### 3.2 Flow rate from the tandem pump

The flow rate of the tandem pump  $Q_T$  is the summation of flow rates from rotating groups A and B, as expressed by (Ye et al., 2014)

$$Q_T = Q_A + Q_B. \quad (16)$$

According to Ericson (2009), the flow rate from each rotating group can be described by its Fourier series coefficients  $a_n$  and  $b_n$  as expressed by

$$Q_A(t) = \frac{Q_0}{2} + \sum_{n=1}^{\infty} [a_n \cos(n\omega_0 t) + b_n \sin(n\omega_0 t)], \quad (17)$$

$$Q_B(t) = \frac{Q_0}{2} + \sum_{n=1}^{\infty} \{a_n \cos[n\omega_0(t + \Delta t)] + b_n \sin[n\omega_0(t + \Delta t)]\}, \quad (18)$$

where  $\Delta t$  denotes the time delay of rotating group B relative to rotating group A, and  $Q_0$  is the mean flow rate, which is given by

$$Q_0 = \frac{2}{T} \int_0^T Q(t) dt. \quad (19)$$

$a_n$  and  $b_n$  are determined from

$$a_n = \frac{2}{T} \int_0^T Q(t) \cos(n\omega_0 t) dt, \quad (20)$$

$$b_n = \frac{2}{T} \int_0^T Q(t) \sin(n\omega_0 t) dt. \quad (21)$$

Thus, the flow rate from the tandem pump is given by

$$Q_T(t) = Q_0 + \sum_{n=1}^{\infty} \{a_n [\cos(n\omega_0 t) + \cos(n\omega_0 t + n\omega_0 \Delta t)] + b_n [\sin(n\omega_0 t) + \sin(n\omega_0 t + n\omega_0 \Delta t)]\}. \quad (22)$$

Note that the value of  $n\omega_0 \Delta t$  plays an important role in the determination of  $Q_T(t)$ . It can be defined that

$$\Delta\varphi = n\omega_0 \Delta t. \quad (23)$$

If  $\delta = 5^\circ$ , then  $\Delta t = T/8$  and  $\Delta\varphi = n\pi/4$ . Thus,

$$\Delta\varphi = \begin{cases} -\frac{7\pi}{4}, & n = 8k - 7, \\ -\frac{3\pi}{2}, & n = 8k - 6, \\ -\frac{5\pi}{4}, & n = 8k - 5, \\ -\pi, & n = 8k - 4, \\ -\frac{3\pi}{4}, & n = 8k - 3, \\ -\frac{\pi}{2}, & n = 8k - 2, \\ -\frac{\pi}{4}, & n = 8k - 1, \\ 0, & n = 8k, \end{cases} \quad k = 1, 2, \dots \quad (24)$$

If  $\delta = 10^\circ$ , then  $\Delta t = T/4$  and  $\Delta\varphi = n\pi/2$ . Thus,

$$\Delta\varphi = \begin{cases} -\frac{3\pi}{2}, & n = 4k - 3, \\ -\pi, & n = 4k - 2, \\ -\frac{\pi}{2}, & n = 4k - 1, \\ 0, & n = 4k, \end{cases} \quad k = 1, 2, \dots \quad (25)$$

If  $\delta = 15^\circ$ , then  $\Delta t = 3T/8$  and  $\Delta\varphi = 3n\pi/4$ . Thus,

$$\Delta\varphi = \begin{cases} -\frac{5\pi}{4}, & n = 8k - 7, \\ -\frac{\pi}{2}, & n = 8k - 6, \\ \frac{\pi}{4}, & n = 8k - 5, \\ \pi, & n = 8k - 4, \\ \frac{7\pi}{4}, & n = 8k - 3, \\ \frac{\pi}{2}, & n = 8k - 2, \\ \frac{5\pi}{4}, & n = 8k - 1, \\ 0, & n = 8k, \end{cases} \quad k = 1, 2, \dots \quad (26)$$

If  $\delta = 20^\circ$ , then  $\Delta t = T/2$  and  $\Delta\varphi = n\pi$ . Thus,



$$\Delta\varphi = \begin{cases} -\pi, & n = 2k - 1, \\ 0, & n = 2k, \end{cases} \quad k = 1, 2, \dots \quad (27)$$

Fig. 9 shows the simulated discharge flow rates with different index angles. The simulation was carried out at the rated condition with a discharge pressure of 28 MPa, a revolution speed of 1500 r/min, and the maximum displacement angle. The index angle was set as 0°, 5°, 10°, 15°, and 20°.

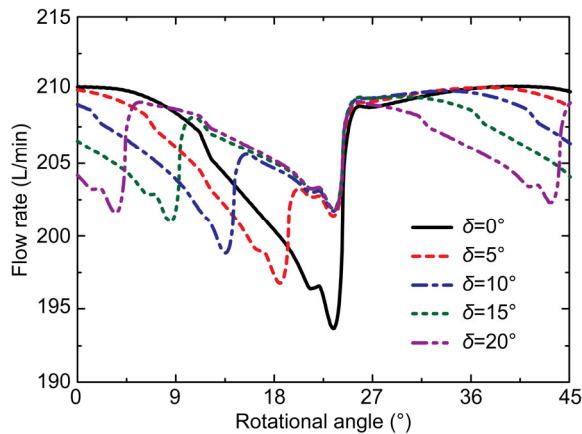


Fig. 9 Discharge flow rates with different index angles

Firstly, the flow rate amplitudes are smaller with larger index angles. The main reason is that the lowest flow rates are higher with larger index angles. The highest flow rates are also smaller with larger index angles. Secondly, the flow rates repeat twice in a period of 40° with an index angle of 20°, while with other index angles they repeat only once. This implies that the frequency contents of flow rates are changed by the use of index angles. The content at the first harmonic is large when  $\delta=0^\circ$ , while the content at the second harmonic is large when  $\delta=20^\circ$ . Fig. 10 shows the frequency spectrums of flow rates with index angles of 0°, 5°, 10°, 15°, and 20°. When  $\delta=0^\circ$ , it is obvious that the flow rate contents appear in every harmonic. When  $\delta=5^\circ$ , the flow rate contents at harmonics which are  $(8k-4)$  multiples of the fundamental frequency (4th, 12th, and 20th) are zero, and those at  $8k$  multiples of the fundamental frequency (8th and 16th) are the same as those with an index angle of zero. The flow rate contents at other harmonics are lower than those with an index angle of zero. When  $\delta=10^\circ$ , the flow rate contents at harmonics which are  $(4k-2)$  multiples of the fundamen-

tal frequency (2nd, 6th, 10th, 14th, and 18th) are zero, and those at odd multiples of the fundamental frequency  $((4k-1)$  and  $(4k-3))$  are lower than those with an index angle of zero. The flow rate contents at harmonics which are  $4k$  multiples of the fundamental frequency (4th, 8th, 12th, 16th, and 20th) are the same as those with an index angle of zero. When  $\delta=15^\circ$ , the flow rate contents at harmonics which are  $(8k-4)$  multiples of the fundamental frequency (4th, 12th, and 20th) are zero, and those at  $8k$  multiples of the fundamental frequency (8th and 16th) are the same as those with an index angle of zero. The flow rate contents with an index angle of 15° at harmonics which are  $(8k-7)$  and  $(8k-1)$  multiples of the fundamental frequency are far smaller than those with an index angle of 5°. When  $\delta=20^\circ$ , the flow rate contents are small at odd harmonics, and the same as those with an index angle of zero at even harmonics. Thus, the flow ripples with an index angle of 20° are smaller than those with an index angle of 0°, 5°, 10°, and 15°, which implies that 20° is the best index angle for reducing the flow ripples of the tandem axial piston pump.

For the tandem axial piston pump, the rotational speed and the discharge pressure level are the same in all working conditions because they are driven by one shaft and share the same suction and discharge ports. But it is difficult for each rotating group to always function at the same displacement angle, mainly because the torque acting on the swash plate causes it to vibrate at high-frequency. Thus, the flow rates from each rotating group can be a little different in some cases.

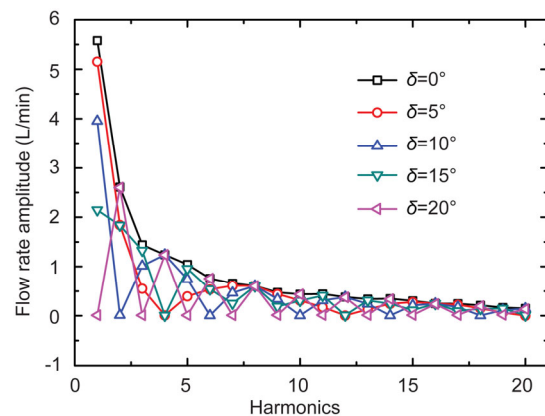
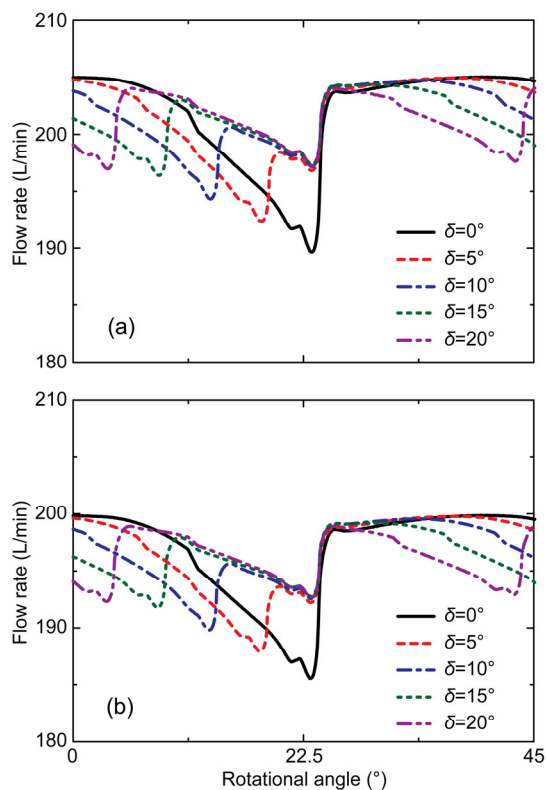


Fig. 10 Frequency spectrum of flow rates with an index angle of 0°, 5°, 10°, 15°, and 20°

Fig. 11 shows the flow rate from the tandem axial piston pump when the flow rates from two rotating groups are a bit different. In this case, the displacement of rotating group A is 100% of the maximum displacement, while that of rotating group B is 95% or 90% of the maximum displacement. Because of the difference in the flow rate produced from rotating group B, the flow rate fluctuates around 205 L/min in Fig. 9, but around 200 and 195 L/min in Fig. 11a and 11b, respectively. Also, the flow rate amplitudes are smaller with larger index angles, and are the smallest with an index angle of  $20^\circ$  (Fig. 9). The reason is similar to that when the two rotating groups produce the same flow rates. But note that  $a_n$  and  $b_n$  from rotating group A are not equal to those from rotating group B. Thus, most of the frequency contents at odd times the fundamental frequency can be cancelled out with an index angle of  $20^\circ$ . This result confirms that an index angle of  $20^\circ$  is the best for reducing the flow ripple of a tandem axial piston pump.



**Fig. 11 Discharge flow rates with different index angles when the two rotating groups are generating different amount of flow rates**

(a)  $Q_A=100\%$ ,  $Q_B=95\%$ ; (b)  $Q_A=100\%$ ,  $Q_B=90\%$

## 4 Sensitivity analysis

Modern axial piston pumps are designed to serve at a wide variety of working conditions, especially at a large scale of pressure levels, speeds, and displacements. It is important to investigate the sensitivity of flow ripple to different working conditions. To determine the sensitivity of flow ripple to different working conditions, simulations were carried out at discharge pressures of 10, 20, and 30 MPa, speeds of 1000, 1500, and 2000 r/min, and displacements of 50%, 75%, and 100% of the maximum displacement with an index angle of  $0^\circ$  or  $20^\circ$ .

### 4.1 Sensitivity to pressure level

Fig. 12 shows the discharge flow rates at pressure levels of 10, 20, and 30 MPa, the maximum displacement, and a revolution speed of 1500 r/min. At 10 MPa, the maximum flow rates are 215.10 and 214.03 L/min, while the minimum flow rates are 206.34 and 209.84 L/min with an index angle of  $0^\circ$  and  $20^\circ$ , respectively. Thus, the flow rate amplitudes are 8.76 and 4.19 L/min, respectively. At 20 MPa, the flow rate amplitudes are 11.79 and 5.26 L/min, and at 30 MPa, they are 17.15 and 7.5 L/min, respectively.

These results reveal a deeper understanding of the relationship between flow rate and discharge pressure level. Firstly, the average flow rates are smaller at higher pressure levels. This is because the leakages across different friction pairs are considered in the simulation model. The leakages are also larger at higher pressure levels. Secondly, the flow rate amplitudes are larger at higher pressure levels. The reason is that the lowest flow rates are smaller at higher pressure levels. As the pressure level increases, more fluid is needed to compress the volume in the piston chamber. Because the compression achieved by the forward motion of piston is almost the same at the same speed and displacement, the compression achieved by the fluid discharging from the discharge port into the piston chamber must be larger at higher pressure levels. Thirdly, the position at which the lowest flow rate appears varies with the variation in pressure level. The rotational angles are smaller at lower pressure levels. This is because less fluid is needed to compress the volume in the piston chamber to reach a lower pressure level. The amount

of fluid discharged into the discharge port is larger at lower pressure levels when the pressure in the piston chamber is higher than that in the discharge port.

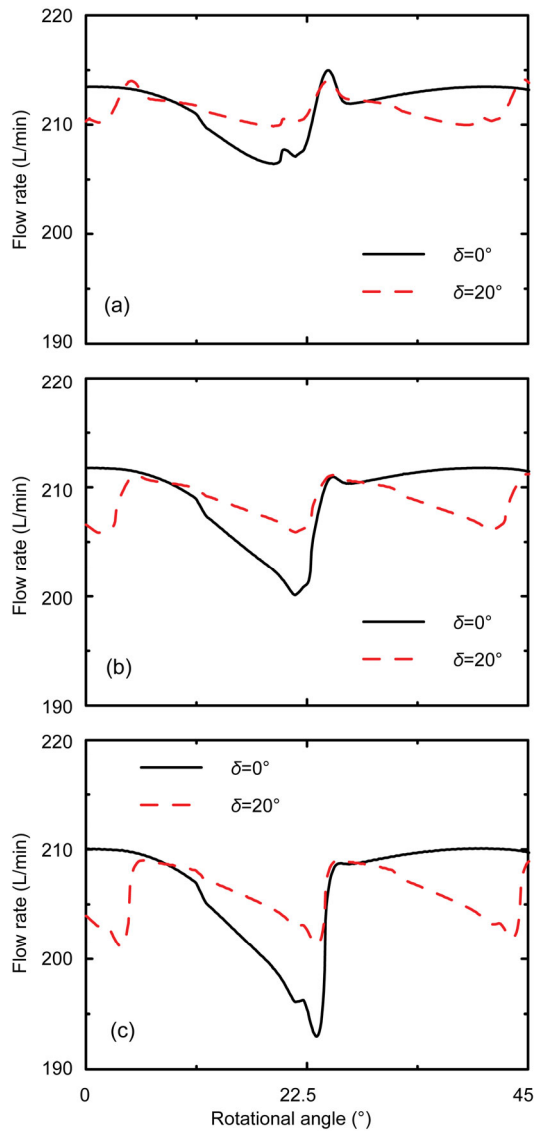


**Fig. 12** Simulated discharge flow rates at different pressure levels

(a) 10 MPa; (b) 20 MPa; (c) 30 MPa

The comparison of the flow rate amplitudes at these three pressure levels indicates that with an index angle of 20° the flow ripples can be reduced by almost 50% compared with an index angle of 0°. This result implies that the sensitivity to pressure level can be reduced significantly with an index angle of 20°.

## 4.2 Sensitivity to speed

Fig. 13 shows the variation in the discharge flow rate at revolution speeds of 1000, 1500, and 2000 r/min, maximum displacement, and a pressure level of 28 MPa. At 1000 r/min, the maximum flow rates are 139.65 and 139.06 L/min, and the minimum flow rates are 130.00 and 134.88 L/min, with an index angle of 0° and 20°, respectively. The amplitudes of the flow rate are 9.65 and 4.18 L/min at 1000 r/min, 16.12 and 7.28 L/min at 1500 r/min, and 35.59 and 11.29 L/min at 2000 r/min, respectively.

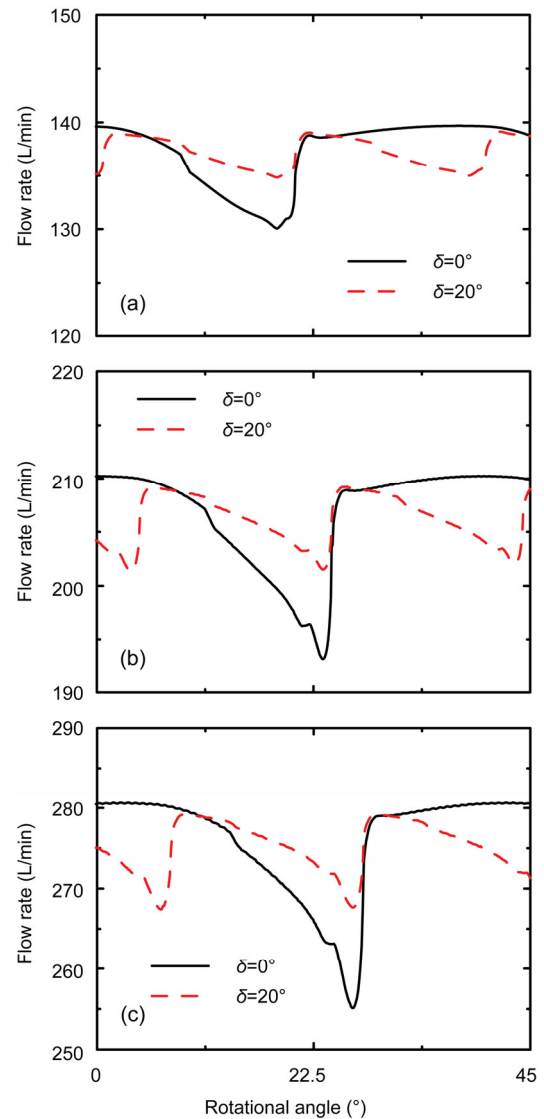


**Fig. 13** Simulated flow rates at different revolution speeds

(a) 1000 r/min; (b) 1500 r/min; (c) 2000 r/min

Thus, the average flow rates and flow rate amplitudes are higher at higher revolution speeds. As the revolution speed increases, the compression produced by the fluid discharging from the discharge port into the piston chamber decreases. More fluid is required to compress the volume in the piston chamber. Thus, more time is needed to compress the fluid in the piston chamber at a higher revolution speed. This result is seen by a comparison of the rotational angles at which the lowest flow rates appear. The rotational angles are larger at higher revolution speeds. For this reason, the throttle areas are larger, and consequently a larger amount of fluid enters into the piston chamber. Also, the flow rate amplitudes are far smaller with an index angle of  $20^\circ$  than those with an index angle of  $0^\circ$  at the investigated speeds. This result reveals that the sensitivity of the flow ripple to speed can also be reduced with an index angle of  $20^\circ$ .

### 4.3 Sensitivity to displacement

Fig. 14 shows the variation in discharge flow rate at displacements of 100%, 75%, and 50% of the maximum displacement, a revolution speed of 1500 r/min, and a pressure level of 28 MPa. At maximum displacement, the flow rate variations are the same as those in Fig. 13b. At 75% displacement, the maximum flow rates are 155.79 and 155.00 L/min and the minimum flow rates are 139.32 and 147.51 L/min. The amplitudes of the flow rates are 16.67 and 7.49 L/min, respectively. At 50% displacement, the maximum flow rates are 101.50 and 100.91 L/min and the minimum flow rates are 86.79 and 94.10 L/min. The amplitudes of the flow rate are 14.70 and 6.81 L/min, respectively. Thus, the flow rate amplitudes are smaller at lower displacements with an index angle of either  $0^\circ$  or  $20^\circ$ . This is because the piston chamber volumes that need to be compressed are smaller at lower displacements and, therefore, less fluid is required to compress the volume in the piston chamber.

Note that the compression produced by the forward motion of the piston is also smaller at a smaller displacement because the displacement of the piston is smaller. Also, the amount of fluid discharging from the discharge port into the piston chamber is smaller. Thus, less time is needed to compress the fluid in the piston chamber. This decreases the throt-

tle area, and consequently decreases the flow rate discharging from the discharge port into the piston chamber. It is also evident that the flow rate amplitude can be greatly reduced with an index angle of  $20^\circ$ .

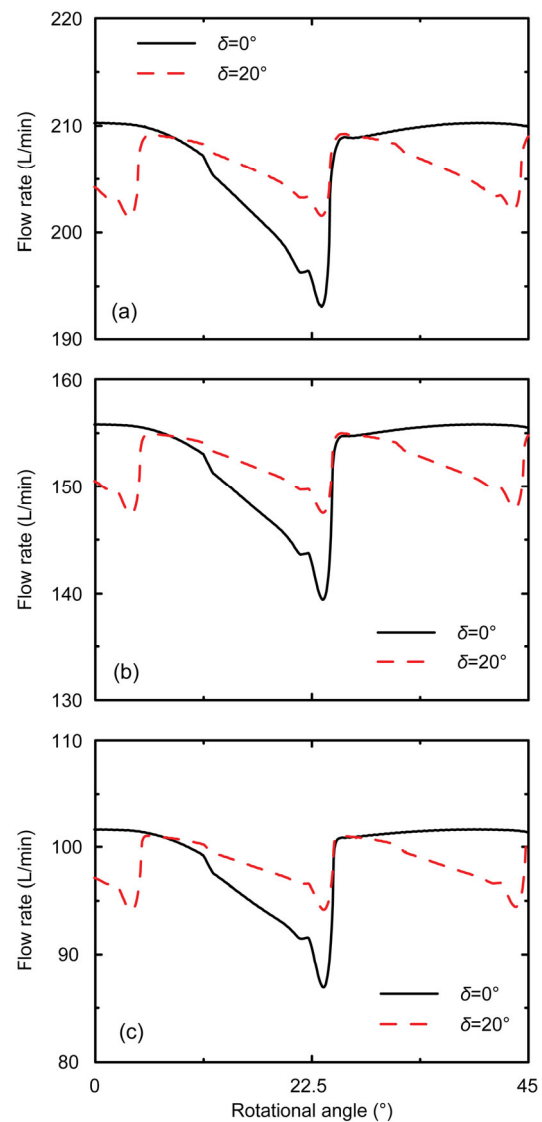


**Fig. 14 Simulated flow rates at different displacements**  
(a) 100%, (b) 75%, and (c) 50% of the maximum displacement

## 5 Conclusions

A dynamic simulation model of an axial piston pump was built to analyze its flow rate characteristics. The analysis was verified by experimental

results using the secondary source method. The simulation model considered the compressibility of fluid and main leakages across different friction pairs, which was capable of capturing the main phenomena in the axial piston pump. The actual flow ripples have frequency contents at each harmonic, while the kinematic flow ripples have frequency contents at even harmonics. The actual flow ripples are far larger than the kinematic flow ripples. Based on these findings, the flow rate of a tandem axial piston pump was obtained on the basis of the flow rate from one rotating group. The findings showed that the best index angle is  $20^\circ$  because the frequency contents of the flow ripples at odd harmonics can be cancelled out. Furthermore, a sensitivity analysis conducted at different pressure levels, speeds, and displacement angles revealed that the sensitivity of the flow ripple can be reduced by almost 50% under a wide variety of working conditions.

## References

- Edge, K.A., Darling, J., 1989. The pumping dynamics of swash plate piston pumps. *Journal of Dynamic Systems, Measurement, and Control*, **111**(2):307-312. [doi:10.1115/1.3153051]
- Edge, K.A., Johnston, D.N., 1990a. The 'secondary source' method for the measurement of pump pressure ripple characteristics. Part 1: description of method. *Proceedings of the Institution of Mechanical Engineers, Part A: Journal of Power and Energy*, **204**(11):33-40. [doi:10.1243/PIME\_PROC\_1990\_204\_006\_02]
- Edge, K.A., Johnston, D.N., 1990b. The 'secondary source' method for the measurement of pump pressure ripple characteristics. Part 2: experimental results. *Proceedings of the Institution of Mechanical Engineers, Part A: Journal of Power and Energy*, **204**(11):41-46. [doi:10.1243/PIME\_PROC\_1990\_204\_007\_02]
- Ericson, L., 2009. Flow Pulsations in Fluid Power Machines—a Measurement and Simulation Study. Licentiate Thesis, Linköping University, Linköping, Sweden.
- Ericson, L., Ölvander, J., Palmberg, J.O., 2007. Flow pulsation reduction for variable displacement motors using cross-angle. Bath Workshop on Power Transmission and Motion Control, Bath, UK, p.103-116.
- Ericson, L., Ölvander, J., Palmberg, J.O., 2008. On optimal design of hydrostatic machines. Proceedings of the 6th International Fluid Power Conference, Dresden, Germany, p.273-286.
- Ericson, L., Johansson, A., Palmberg, J.O., 2009. Noise reduction by means of non-uniform placement of pistons in a fluid power machine. ASME 2009 Dynamic Systems and Control Conference, Volume 2, California, USA, p.381-388. [doi:10.1115/DSCC2009-2645]
- Fiebig, W., 2001. Schwingungs und Geräuschverhalten der Verdrängerpumpen und Hydraulischen Systeme. PhD Thesis, University of Stuttgart, Stuttgart, Germany (in German).
- Huang, J.H., Zhao, H., Quan, L., et al., 2014. Development of an asymmetric axial piston pump for displacement-controlled system. *Proceedings of the Institution of Mechanical Engineers, Part C: Journal of Mechanical Engineering Science*, **228**(8):1418-1430. [doi:10.1177/0954406213508385]
- ISO (International Organization for Standardization), 1996. Hydraulic Fluid Power-Determination of Pressure Ripple Levels Generated in System and Components. Part 1: Precision Method for Pumps, ISO 10767-1:1996. ISO.
- Ivantysyn, J., Ivantysynova, M., 2003. Hydrostatic Pumps and Motors: Principles, Design, Performance, Modelling, Analysis, Control and Testing. Akademia Books International, New Delhi, India, p.125-135.
- Johansson, A., Andersson, J., Palmberg, J.O., 2001. Effects of cross-angle on piston forces and bending moments in axial piston pumps. The 7th International Symposium on Fluid Control, Measurement and Visualization, Sorrento, Italy, p.1-10.
- Johansson, A., Andersson, J., Palmberg, J.O., 2002. Optimal design of the cross-angle for pulsation reduction in variable displacement pumps. Bath Workshop on Power Transmission and Motion Control, Bath, UK, p.319-334.
- Johansson, A., Andersson, J., Palmberg, J.O., 2003. Influence from the cross-angle on piston forces and bending moments in variable hydraulic piston pumps. Technical Report No. LiTH-IKP-R-1391, Linköping University, Sweden.
- Johansson, A., Ölvander, J., Palmberg, J.O., 2007. Experimental verification of cross-angle for noise reduction in hydraulic piston pumps. *Proceedings of the Institution of Mechanical Engineers, Part I: Journal of Systems and Control Engineering*, **221**(3):321-330. [doi:10.1243/09596518JSCE208]
- Landsberger, B., 2003. Using the ideal function concept for machine noise control. *The Journal of the Acoustical Society of America*, **114**(4):2440-2440. [doi:10.1121/1.4779199]
- Ma, J.E., Fang, Y.T., Xu, B., et al., 2010. Optimization of cross angle based on the pumping dynamics model. *Journal of Zhejiang University-SCIENCE A (Applied Physics & Engineering)*, **11**(3):181-190. [doi:10.1631/jzus.A0900417]
- Manring, N.D., 2003. Valve-plate design for an axial piston pump operating at low displacements. *Journal of Mechanical Design*, **125**(1):200-205. [doi:10.1115/1.1541632]
- Manring, N.D., Mehta, V.S., Raab, F.J., et al., 2007. The shaft torque of a tandem axial-piston pump. *Journal of Dynamic Systems, Measurement, and Control*, **129**(3):367-371. [doi:10.1115/1.2719785]



- Mehta, V.S., 2006. Torque Ripple Attenuation for an Axial Piston Swash Plate Type Hydrostatic Pump: Noise Considerations. PhD Thesis, University of Missouri-Columbia, USA.
- Nafz, T., Murrenhoff, H., Rudik, R., *et al.*, 2012. Noise reduction of hydraulic systems by axial piston pumps with variable reversing valves. The 8th International Fluid Power Conference, Aachen, Germany, p.1-12.
- Seeniraj, G.K., Ivantysynova, M., 2011. A multi-parameter multi-objective approach to reduce pump noise generation. *International Journal of Fluid Power*, **12**(1):7-17. [doi:10.1080/14399776.2011.10781018]
- Xu, B., Zhang, J.H., Yang, H.Y., 2013. Simulation research on distribution method of axial piston pump utilizing pressure equalization mechanism. *Proceedings of the Institution of Mechanical Engineers, Part C: Journal of Mechanical Engineering Science*, **227**(3):459-469. [doi:10.1177/0954406212462336]
- Xu, B., Sun, Y.H., Zhang, J.H., *et al.*, 2015. A new design method for the transition region of the valve plate for an axial piston pump. *Journal of Zhejiang University-SCIENCE A (Applied Physics & Engineering)*, **16**(3): 229-240. [doi:10.1631/jzus.A1400266]
- Ye, S.G., Xu, B., Zhang, J.H., 2014. Investigation into the

effects of index angle on fluidborne noise and structure-borne noise of a tandem axial piston pump. 8th FPNI PhD Symposium on Fluid Power, Lappeenranta, Finland, p.V001T01A002. [doi:10.1115/FPNI2014-7815]

## 中文概要

**题目:** 转位角对串联式轴向柱塞泵流量脉动的影响

**目的:** 探索转位角对串联泵出口流量脉动的影响, 揭示转位角对流量脉动的影响机理, 获得最佳转位角以减小流量脉动, 以及探索转位角对工况的敏感性。

**方法:** 1. 建立基于单柱塞腔模型的单柱塞泵模型, 求解其出口流量脉动特性; 2. 研究不同转位角下串联泵的出口流量脉动, 优选转位角; 3. 对比不同转位角下出口流量脉动对工况的敏感性。

**结论:** 1. 对于单个转子使用九柱塞的串联式轴向柱塞泵, 最佳转位角是  $20^\circ$ , 因该角度可消除流量脉动在奇数阶次下的幅值; 2. 在大范围工况下, 转位角为  $20^\circ$  时可减小约 50% 的流量脉动。

**关键词:** 轴向柱塞泵; 流量脉动; 转位角; 敏感性分析